Green Chemistry

Accepted Manuscript

ROYAL SOCIETY OF CHEMISTRY

www.rsc.org/greenchem

Green Chemistry RSCPublishing

ARTICLE

Anion Exchange Capacity of Biochar

M. Lawrinenko[a] and D. A. Laird[a]

[a] Department of Agronomy, Iowa State University, Ames, Iowa, United States

Biochar has gained recent interest as a soil amendment and agent for carbon sequestration. Some biochars have significant levels of anion exchange capacity (AEC), which may reduce leaching of anionic nutrients in soil. Little is known about the nature of anion exchange sites on biochar surfaces and what production conditions promote AEC in biochar. We report that the AEC of biochars produced from four feedstocks (maize stover, cellulose, alfalfa meal, and albumin) ranged from 0.602 to 27.76 cmol Kg^{-1} and increased with decreasing pH ($p < 0.0001$) and peak pyrolysis temperature. A cellulose biochar, composed almost entirely of C, H, and O, exhibited significant AEC at pH 8 suggesting that pH independent O containing functional groups contribute AEC. Fourier transform infrared spectroscopy revealed a prominent 1590 cm^{-1} band, which we attribute in part to $C\text{-}O^{+}$ stretching in oxonium heterocycles. Both the C1s and O1s x-ray photoelectron (XPS) spectra of the biochars provide additional evidence for oxonium heterocycles. The N1s XPS spectra of albumin biochars indicated the presence of pyridinic groups. We conclude that oxonium functional groups contribute pH independent AEC and that both pyridinic functional groups and non-specific proton adsorption by condensed aromatic rings contribute pH dependent AEC to biochars.

Cite this: DOI: 10.1039/x0xx00000x

Received ooth April 2015,

Accepted ooth January 2012

DOI: 10.1039/x0xx00000x

www.rsc.org/

1. Introduction

Pyrolysis, heating in low-oxygen conditions, thermally converts biomass into bio-oil, syn-gas, and a carbon enriched solid residue known as biochar. There is increasing interest in the use of biochar as a soil amendment[1], because of evidence demonstrating increased soil fertility through the reduction of leaching losses of nutrients such as nitrate and phosphate[2,3], amelioration of soil acidity[4], contribution to the cation exchange capacity (CEC) of soil[5], and many other intervening mechanisms.

Biochar's chemical and physical properties vary widely and are dependent on the nature of the feedstock and production conditions. It is well known that carbon content and aromaticity both increase with highest treatment temperature (HTT)[6-9]. Aromaticity accounts for the recalcitrance of biochar in soils as condensed aromatic carbon is resistant to oxidation[10]. Oxygen (O) containing alcohol, carbonyl, and carboxylate functional groups are generally believed to contribute to biochar cation exchange capacity (CEC) because they may carry a negative charge and serve as Lewis bases for the sorption of cations. Heteroatom containing chemical functional groups in biochar also influence surface properties as they are generally polar and provide sites for hydrogen bonding, ion-dipole, and dipole-dipole interactions[11]. By contrast, the carbon rich surfaces of biochar are hydrophobic and provide sorption sites for non-polar moieties. Thus the distribution and density of various functional groups greatly influence the relative hydrophilic/hydrophobic nature of biochar surfaces. While the origin of CEC in biochars and the hydrophobic/hydrophilic nature of biochar surfaces are mechanistically well understood, little is known about the anion exchange capacity (AEC) of biochar.

Only a few studies have reported on the AEC of biochar. Mukherjee et al. (2011)[12] were not able to detect AEC for oak (*Quercus lobata*), pine (*Pinus taeda*) and grass (*Tripsacumfloridanum*) biochars produced at 400 and 650 °C under N_2 purge. They did measure isoelectric points between pH 2 and 3 suggesting that AEC might exist under very acidic conditions. By contrast, Inyang et al., (2010)[13] measured AEC values of 6.64 and 11.19 cmol Kg^{-1} for biochars made by pyrolysis at 600 °C from sugarcane bagasse and anaerobically digested bagasse, respectively; and Silbr et al. (2010)[14] reported an AEC of 15.4 cmol Kg^{-1} that was stable over the pH 4 to 8 range for a maize stover biochar produced at 500 °C. Cheng et al. (2008)[15] measured AECs ranging from 1.8 to 8.4 cmol Kg^{-1} for freshly prepared biochars and biochars incubated for 12 months at 30 °C; but did not detect AEC for biochars recovered from historic kiln sites or fresh biochars that had incubated for 12 months at 70 °C.

Little is known about the nature of anion exchange sites in biochar. Boehm (1994)[11] reported that basic surface oxides readily form on the surfaces of activated carbons and carbon blacks with oxidation. He suggested that these basic surface oxides could be pyrones and proposed that oxonium heterocycles could be produced by acid reduction of pyrones. Huang et al. (2004)[16] reported increased bromate removal from drinking water by activated carbons with greater basic surface oxide content and higher isoelectric points, illustrating the potential for basic surface oxides to contribute AEC. Alternatively, the π-electrons of aromatic carbon may be sufficiently basic to bind protons abstracted from aqueous acid solutions[11,17] resulting in delocalized positive charge. Any AEC resulting from protonated aromatic structures should be pH dependent and fully reversible at high pH. Ahmad et al.[18] attributed AEC to protonation of carboxylate and/or ether moieties at low pH, citing studies on biochar mediated heavy

metal-oxyanion sorption. This mechanism, however, does not seem plausible as the pKas of protonated and positively charged benzoic acids and phenyl ethers are in the -6 range[19]. Other than the work by Boehm, there are no reports on the nature of AEC sites on biochar surfaces, and no reports on the stability of biochar AEC beyond that of Cheng et al. (2008)[15]. However, it is evident that AEC can be found in some biochars and that feedstock and pyrolysis conditions may influence the AEC of biochars.

We hypothesized that nitrogen (N) and oxygen (O) heterocycles are the functional groups responsible for AEC in biochars. Previous studies have indicated the presence of pyridinic and pyrrolic / pyridone forms of N in biochars[20-22]. While pyrrolic and pyridone groups are neutral, pyridinic groups protonate at pHs below their pKa and carry a +1 formal charge and therefore could be a source of AEC. Other studies reported evidence of O heterocycles in maize stover[23] and rice straw[8] derived biochars using ^{13}C nuclear magnetic resonance (NMR) spectroscopic analysis. Heterocyclic O is electrically neutral in the case of cyclic ethers and pyrones or may carry a pH independent +1 formal charge when sp^2 hybridized as in the structure of pyrylium, an oxonium heterocycle. Therefore oxonium groups are another potential source of AEC. Biochars are commonly known to contain significant amounts of O and some N, yet the functional forms of these elements in biochar are not completely understood and there is a lack of knowledge as to how pyrolysis conditions influence the development of specific functional groups in biochar.

It was the purpose of this study to determine whether O and/or N heterocycles are present in biochar and if these structures contribute AEC to biochar. We also sought to determine whether the AEC of biochar is influenced by HTT and how the chemical nature of the biomass feedstock used to produce biochar influences AEC.

2. Materials and Methods

2.1.1 Biochar preparation

Biochars were prepared by slow-pyrolysis of the feedstock (500 g) in a muffle furnace using a program that quickly brought the furnace temperature to 100 °C below the desired peak temperature, held the temperature constant for two hours, elevated the temperature at 0.5 °C min^{-1}, and then held the temperature at HTTs of 500 °C or 700 °C for 1 hr. Bulk biochar samples were produced from albumin (egg powder, Acros) alfalfa meal, ground maize stover, and cellulose powder (Sigma-Aldrich) under a 40 mL min^{-1} N_2 purge in a stainless steel box. Feedstocks were not screened for particle size, however, the biochars were gently crushed to pass through a No. 12 sieve (hole size of 1680 μm), mixed and transferred to 1 L plastic storage bottles. Mass yield was recorded.

2.1.2 Biochar treatments

Biochar samples were given various pretreatments before analysis, hereafter those treatments are referred to as *untreated, dialyzed, HCl treated,* and *HCl/HF treated*. Untreated samples were freshly prepared biochar samples. Dialyzed samples were prepared by dialyzing slurries of untreated biochar (using Spectra / POR® MW6-8000, 32mm dialysis tubing) against deionized (DI) water until steady state conductivity of bath solution was achieved. HCl treated samples were subsamples of untreated biochar shaken in 1 M HCl for 24 hours on an oscillating shaker at room temperature. pH was measured to confirm excess acidity (pH <2). Samples

were then rinsed with Milli-Q water and filtered across 0.45 μm Teflon filters under vacuum until the conductivity of the rinsate was below 5 μS cm^{-1}. Samples were then dried in a convection oven for 24 hours at 105 °C and ground in a puck mill for two minutes. HCl/HF treated samples were subsamples of the HCl treated biochars that were further shaken in 0.1 M HCl and 0.3 M HF for 36 hours on an oscillating shaker at room temperature, subsequently rinsed with Milli-Q water, and filtered across 0.45 μm Teflon filters under vacuum until the conductivity of the rinsate was below 5 μS cm^{-1}. Samples were then dried in a convection oven at 105 °C for 24 hours. This HCl/HF treatment was adapted from the International Humic Substance Society method for removal of silica from soil humic acid samples [23].

2.2 Biochar characterization

2.2.1 Elemental, surface area, particle density, ash, and pH analyses

Untreated biochar samples were analyzed to determine total C, N, H, and S content, ash content, specific surface area, and particle density. Oxygen content was computed as the difference between the sum of C, N, H, and S mass fractions from unity for biochars produced from cellulose and the HCl/HF treated albumin biochars. Elemental analyses were performed in duplicate using an Elementar Vario Micro Cube combustion analyzer with argon as a carrier gas. Specific surface area was measured using the Brunauer–Emmett–Teller (BET) method with a NOVA 4200e gas adsorption analyzer (Quantachrome Instruments). High purity nitrogen (>99.999%) gas was used as the adsorbent. Particle density measurements were made using a helium pycnometer (Pentapycnometer, Quantachrome Instruments). Ash content of untreated biochars was determined gravimetrically following combustion at 550 °C for 48 hours of 1 to 2 g of oven dried (105 °C for 24 hours) samples in forged ceramic crucibles. Ash analysis was performed in duplicate. Ash content of HCl and HCl/HF treated albumin derived biochars was determined thermogravimetrically using a TA Instruments Discovery TGA. Samples (20mg) were heated in air from ambient temperature to 1000 °C at 10 °C per minute. pH of biochars in 1:20 (wt/wt) DI water suspensions was measured with a pH meter and a glass electrode after being shaken for three days on an oscillating shaker.

2.2.2 FTIR Analysis

FTIR spectra of biochar samples were obtained with a Nicolet 560 Magna - IR spectrophotometer using the diffuse reflectance accessory. Spectra were measured from 4000 to 400 cm^{-1} at a resolution of 4 cm^{-1} and a total of 200 scans were averaged to produce the final spectrum. Biochars were co-ground with spectroscopy grade KBr in a SPEX 5100 mixer mill at 1% wt/wt in KBr. Assignment of vibrational modes was based on published tables [24]. Spectra of model compounds of 2,4,6 triphenylpyrylium hydrogensulfate (Tokyo Chemical Industry Co. LTD, Lot# FILo1-NVKL) and 1,3,5-triphenylbenzene (Alfa Aesar, Lot# 10184587) were obtained from samples prepared as biochars samples described above.

2.2.3 X-ray Diffraction Analysis

X-ray diffraction (XRD) analysis of biochar samples was performed with a Siemen D5000 x-ray diffractometer using Cu Kα radiation generated at 40 KV and 30 mA. Step scan mode was used with a step size of 0.05° 2θ and a dwell time of 7 seconds per

step. A scintillation counter detector with fixed 0.15° divergence and 1.0° anti-scattering slits was used. Random powder mounts of biochars were analyzed at ambient temperature and humidity.

2.2.4 X-ray Photoelectron Spectroscopic Analysis

X-ray photoelectron spectroscopy (XPS) was performed on untreated biochars using a Physical Electronics 5500 Multitechnique spectrometer with a standard aluminum source. Analysis spot size was 2mm x 2mm. Samples were mounted on double sided tape. Spectra were shifted relative to the carbon maximum at 284.7 eV. Deconvolution of N1s spectra of albumin derived biochars was performed with Gaussian fit and Shirley background using Multipak software V6.1A with N 5 and 6 member heterocycle assignments made by the method described by Darvell et al. (2012)[20].

2.2.5 AEC Analysis

Anion exchange capacity was measured in triplicate at pHs of 4, 6, and 8 using bromide as an index anion. Milli-Q water was used in all steps of AEC measurement. One gram samples of dialyzed biochar were adjusted to stable pH using either NaOH or HBr. Once stable pH was achieved (within 2 weeks), 2 mL of 1 M KBr was added to the suspension, shaken for two days, then rinsed on 0.45 µm Teflon filter paper until conductivity of the rinsate was below 5 µS cm^{-1}. Biochar was quantitatively transferred back into sample bottles and combined with 2 mL of 2.5 M $CaCl_2$ and 50 mL water. Samples were then returned to the shaker for two days. Biochar slurries were subsequently diluted to 200 mL in a volumetric flask. A portion of this was filtered through an IC Acrodisk® 25 mm syringe filter with 0.45 µm Supor® PES membrane (PALL Life Sciences) and 10.0 mL of filtrate was diluted to 100 mL. This final solution was assayed for bromide using a Dionex® 1100 ion chromatograph with an ASRS 300 4 mm conductivity detector. The mobile phase was 8 mM Na_2CO_3 / 1 M $NaHCO_3$. The method was run at 0.7 mL min^{-1} using an IonPac® AG14A 5 µm 3 x 30 mm guard column and an IonPac® AS14A 5 µm 3 x 150 mm analytical column. A best fit five point calibration curve was used with a standard bracket every 12 sample injections. The calibration standards were prepared by dilution of a certified 7 anion reference standard purchased from Dionex®. Each sample was analyzed in duplicate.

2.3 Statistical Analysis

Statistical analysis of AEC measurements was performed using SAS 9.3 (GLIMMIX, SAS 9.3, SAS Institute Inc., Cary, NC, USA). Data was treated using a 2-way ANOVA in a randomized complete block design in which individual biochars were treated as blocks. Main effects of pH and block were assessed as well as the pH by biochar interaction effect.

3. Results and Discussion

3.1 Anion exchange capacity

Measured AEC values for the studied biochars ranged from 0.60 to 27.8 cmol Kg^{-1} (Table 1). The AEC of the 700°C biochars was consistently higher than the AEC of the 500°C biochars produced from the same feedstock. The effect of feedstock on AEC was less obvious, but in general the maize stover and cellulose biochars had higher AEC values than the alfalfa and albumin biochars. Because only one batch of biochar was produced for each combination of HTT and feedstock it was not possible to use statistical

analysis to test the direct effects of HTT or feedstock on AEC. However, we were able to use statistical analysis to assess the effect of pH on AEC as independent subsamples of each biochar were equilibrated at each pH.

AEC of the biochars increased significantly ($p < 0.0001$) with decreasing pH (Table 1), averaging 2.5, 7.4, and 18.0 cmol kg^{-1} at pH 8.0, 6.0, and 4.0, respectively. The increase in AEC with decreasing pH is consistent with protonation of hetero-N in 6-member rings; pyridinic groups. The pKa of pyridine is 5.2 and pyridinic groups in condensed aromatic C are anticipated to have pKa values in a similar range, hence any pyridinic groups present in the biochars equilibrated at pH 4 ought to have been protonated and contributing to AEC. However, the maize stover and cellulose biochars, which contain little and no N, had higher AEC values than the alfalfa and albumin biochars, which have medium and high levels of N, respectively (Tables 1 and 2). This observation indicates that protonated pyridinic functional groups could not have been the primary source of AEC in the maize stover and cellulose biochars. Proton abstracted from hydronium to the basal planes of aromatic carbon also probably contributed AEC at acidic pH[11,16]. Furthermore, the AEC methodology measured Br^- that was retained by the biochar, but was not designed to measure OH^- groups that may also have been retained by anion exchange sites. Thus the decrease in measured AEC with increasing pH can also be partially explained by competition between OH^- and Br^- for anion exchange sites, especially at pH 8 where the concentration of OH^- is non-negligible. However, none of the above mechanisms or processes can explain the non-zero AEC measured at pH 8 where both pyridinic groups and the basal planes of aromatic carbon should have been deprotonated and therefore not contributing to AEC. Oxonium heterocycles, by contrast, could provide AEC at pH 8 as oxonium groups carry a pH independent positive charge.

Table 1. Anion exchange capacity of biochars produced from three feedstocks at 500 and 700 °C HTT. Analyses performed in triplicate and data is presented as average (standard deviation).

Feedstock	HTT (℃)	pH 4 (cmol kg^{-1})	pH 6 (cmol kg^{-1})	pH 8 (cmol kg^{-1})
Albumin	500	14.7 (1.05)	2.45 (0.464)	1.65 (0.948)
Albumin	700	15.5 (1.71)	5.95 (1.10)	2.32 (0.881)
Alfalfa	500	10.9 (2.46)	3.1 (0.28)	0.94 (0.34)
Alfalfa	700	25.8 (4.08)	9.6 (1.07)	2.1 (0.87)
Cellulose	500	7.8 (1.94)	2.6 (0.21)	0.60 (0.37)
Cellulose	700	24.2 (5.94)	18.1 (8.66)	4.1 (0.18)
Maize Stover	500	17.5 (5.81)	3.8 (0.66)	1.0 (0.21)
Maize Stover	700	27.8 (9.10)	13.8 (4.22)	7.2 (1.39)

3.2 Biochar physical and compositional properties

Pyrolysis temperature and biomass composition influence the chemical and physical characteristics of the studied biochars (Table 2). Particle density increased while yields decreased slightly with HTT for all biochars. These trends are due to loss of labile elements such as H, N, S and O, which are preferentially volatilized relative to C with increasing HTT. Other constituent atoms

present in the biomass feedstock, particularly metals, are concentrated in the biochar fraction during pyrolysis, as reflected by increases in the ash content with HTT (Table 2), which is consistent with other reports[18,25,26]. The ash is composed primarily of silica, salts, and metal carbonates, although some metal oxides and hydroxides also may form during biomass pyrolysis[26,27]. The pH of biochar suspensions ranged from 8.3 for the 500°C cellulose biochar to 12.7 for the 700°C albumin biochar and was either constant or increased slightly with HTT.

The specific surface area of these biochars ranged from 0.9 to 321 m^2 g^{-1} (Table 2) and was clearly influenced by both feedstock (cellulose > maize stover > alfalfa > albumin) and HTT (700°C > 500°C), however there was no clear relationship between specific surface area and AEC. The ratio of AEC to specific surface area (AEC/SSA) varied substantially among the various biochars (Table S1). Biochars produced from albumin exhibited very low specific surface area (Table 2), and as a result the albumin 500°C HTT biochar had the highest AEC/SSA ratio and the cellulose 500°C HTT biochar, which had the highest SSA, had the lowest AEC/SSA ratio. The AEC/SSA ratios for these two biochars differed by two orders of magnitude at all three pHs. The AEC/SSA ratios consistently decreased with increasing pH, but there was no clear pattern for the effect of HTT or feedstock on AEC/SSA ratios. The variation in AEC/SSA ratios indicates that AEC of biochars is not a linear function of surface area as measured by the BET method using N_2 as the probe molecule. It should be noted, however, that N_2 is not an ideal probe for assessing the effect of biochar surface area on AEC as water and exchangeable anions may not explore the surfaces of biochar to the same extent as N_2.

Composition of the organic fraction of biochar is influenced by pyrolysis temperature. Generally the 700 °C HTT biochars contained more C and less N and H than the 500 °C HTT biochars (Table 2), which is consistent with the literature[6,7,8,10]. Oxygen content of the organic fraction is not calculable by difference for the untreated albumin, alfalfa, and maize stover biochars as O is partitioned between the condensed aromatic carbon phase and inorganic mineral phase.

Table 2. Properties of the untreated biochars, including mass yields, elemental composition, pH, ash content, specific surface area, and particle density.

			Element Content (%)								
Feedstock	HTT (°C)	Yield (%)	C	N	H	S	O	pH	Ash (%)	BET-N_2 (m^2/g)	Particle Density (g/cm^3)
Albumin	500	24.2	60.81	10.8	2.91	0.34	a	12.5	19.49	0.9	*
Albumin	700	21.2	62.05	8.39	1.71	0.34	a	12.7	26.36	2.6	*
Alfalfa	500	29.8	66.03	3.4	2.43	0.18	a	10	28.84	39	1.61
Alfalfa	700	29.0	68.8	3.23	1.45	0.25	a	10	30.89	176	1.9
Cellulose	500	27.9	84.8	0	2.98	0.08	10.82	8.3	0.87	321	1.34
Cellulose	700	26.0	90.3	0.01	1.72	0.12	6.12	8.6	0.92	229	1.68
Maize Stover	500	31.5	75.45	1.48	2.67	0.08	a	10.1	20.03	150	1.56
Maize Stover	700	29.8	77.54	1.23	1.48	0.13	a	10.2	21.93	259	1.74

[a] cannot be determined from the methods used. * not measured.

Figure 1 presents XRD patterns of HCl / HF treated 700 °C HTT biochars. Despite treatment with both 1M HCl for 24 hr, grinding, and 0.1 M HCl and 0.3 M HF for 36 hours; quartz, sylvite, and calcite peaks were detected in the XRD patterns of the alfalfa and maize stover biochars. These results suggest that some inorganic phases were occluded within the C matrix of these biochars and were not able to interact with the acid solutions. The acid treatments, by contrast, did remove all detectable ash from the albumin biochars as evidenced by negligible (<0.5%) ash content and the lack of evidence for crystalline mineral phases in the XRD patterns of the acid-treated albumin biochars. The cellulose employed in this study had negligible ash content (Table 2) and there was no evidence of inorganic phases in the XRD patterns of the cellulose biochars. Therefore, we infer that all O in the untreated cellulose biochars and the HCl / HF treated albumin biochars, as calculated by mass difference, is structurally incorporated into the condensed aromatic C matrix of these biochars. The O content of the 500°C and 700°C HTT samples were 10.82 % and 6.12 % for the untreated cellulose biochar and 8.41 % and 11.84 % for the HCl / HF treated albumin biochars, respectively. FTIR spectroscopy indicated the HCl / HF treated albumin biochars contained more OH and COOH groups than the untreated albumin biochars suggesting that some of the O in the acid treated albumin biochars was acquired during the HCl and/or HCl / HF treatments. These changes are discussed later along with the other FTIR interpretations.

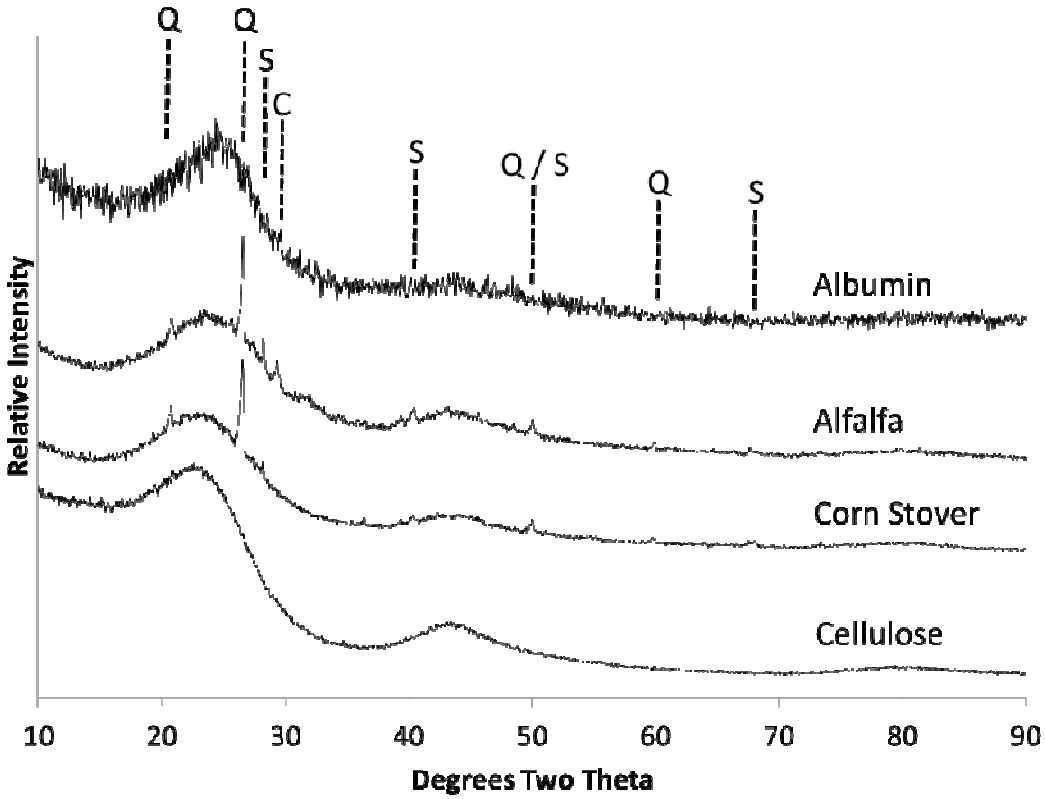

Figure 1. X-ray diffraction patterns of HCl / HF treated biochars produced at a HTT of 700 °C with crystalline assignments: Q = Quartz, S = Sylvite, and C = Calcite

3.2 FTIR interpretation

Infra-red spectroscopy was used to investigate structural forms of N and O in the studied biochars. Infra-red spectra of the dialyzed and HCl treated 500 °C HTT biochars (Figures 2 & 3) show little evidence of hydroxyl and amine functionality which should be evident as bands in the 3200-3500 v_{max}/cm^{-1} range. Some evidence for aromatic C-H stretching was observed based on the small peaks centered at 3050 v_{max}/cm^{-1}. A weak band at 2170 v_{max}/cm^{-1} is observed in the spectra of the albumin and alfalfa meal biochars and is suggestive of isonitrile character; however acid treatment eliminated this feature. There is little evidence of the C-O stretch for ethers which should be observed between 1000 and 1300 v_{max}/cm^{-1}. The carbonyl C=O stretch at 1700 v_{max}/cm^{-1} is one of the most prominent vibrations observed in infra-red spectroscopy, yet the weak intensity of this band in these spectra indicates only minor contribution of carbonyl groups to the surface chemistry of the 500 °C biochars. Thus it is difficult to account for the relatively high levels of structural O (10.82% and 8.41 %) found in the 500 °C cellulose and albumin biochars based on the spectroscopic evidence for negligible levels of hydroxyl and low levels of carbonyl groups.

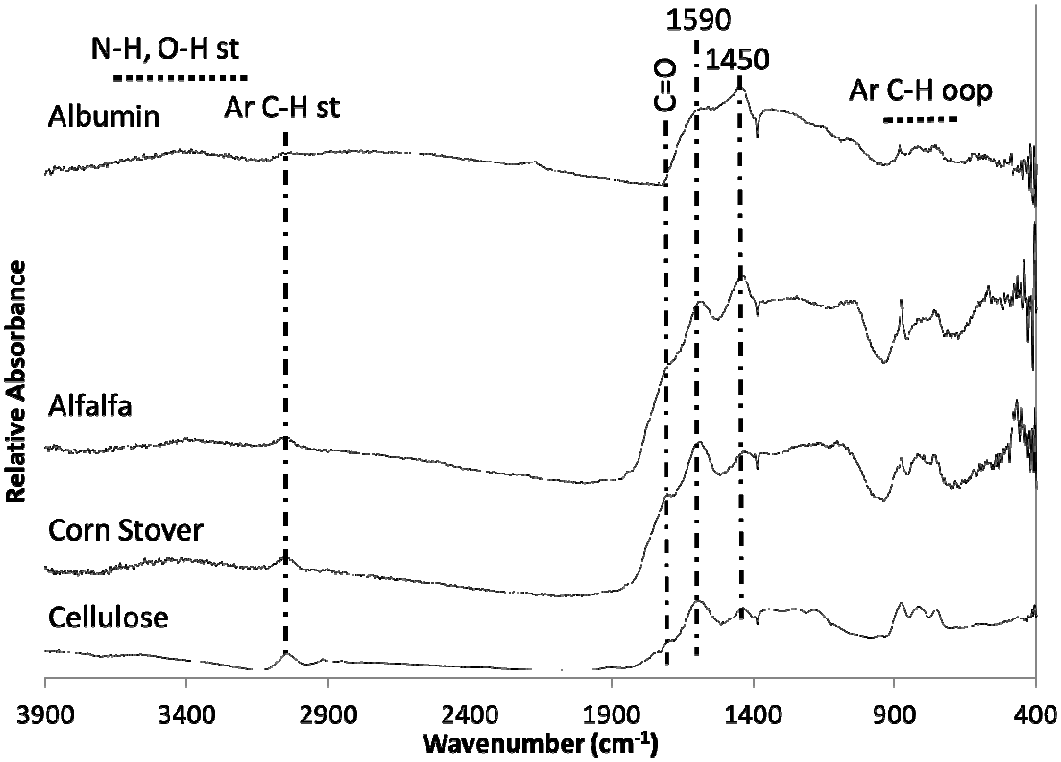

Figure 2. FTIR spectra of dialyzed biochars slow pyrolyzed at a HTT of 500 °C. N-H, O-H st indicate hydroxyl or amine/amide H-stretching bands; Ar C-H st is aromatic C-H stretching, C=O is carbonyl stretching, and Ar C-H oop indicates aromatic C-H out of plane vibrations.

The peak at 1450 v_{max}/cm^{-1} is assigned to aromatic C-C symmetric stretching. This assignment is consistent with the reduced vibrational frequency of C-C aromatic symmetric stretching observed with increased polynucleation of aromatic compounds. The origin of the prominent 1590 v_{max}/cm^{-1} band observed in the spectra for all of the 500 °C biochars is less clear as several structures could potentially contribute to it. The 1700 v_{max}/cm^{-1} carbonyl band can shift to 1600 v_{max}/cm^{-1} when carboxylate groups are associated with inorganic cations such as Na^+ or K^+. That the intensity of the 1590 v_{max}/cm^{-1} band was not diminished when the cellulose biochar was washed with acid (Figure 3), however indicates that carboxylates are not primarily responsible for this band, as the acid washing treatments should have replaced any inorganic cations associated with carboxylate groups by protons. Asymmetric C-C stretching also contributes to this band; however, the intensity of the 1590 v_{max}/cm^{-1} band observed in the spectra of the maize stover and alfalfa meal biochars which have lower carbon content in comparison to the biochar derived from cellulose alludes to the presence of other bonding structures.

Oxonium heterocycles present in the biochar samples ought to be evident in FTIR spectra by a C-O^+ stretching band. The C-O^+ stretch exhibits strong absorbance in the 1600-1640 v_{max}/cm^{-1} region in model compounds, with decreased energy of vibration observed in compounds of greater substitution[28] and was observed at 1622 v_{max}/cm^{-1} in the spectrum of 2,4,6-triphenylpyrylium hydrogensulfate (Figure S1). Aromatic C-heteroatom stretching generally vibrates at lower energy than aromatic C-C stretching, due to increased mass of the heteroatom relative to C. The very strong 1600-1640 v_{max}/cm^{-1} vibration observed in model oxonium compounds is due to larger bond order in C-O^+ bonds[29] as compared to C-C benzylic and other C-heteroatom bonds as the smaller atomic radius of O^+ creates a more electronegative nucleus resulting in shorter C-O^+ bond length and a large dipole change during vibration. Oxonium heterocycles in biochar are components of large polynuclear aromatic carbon structures. The positive charge associated with the oxonium heteroatom is delocalized through a large molecular orbital structure, creating a lower effective charge at the hetero oxygen atom, and resulting in longer C-O^+ bonds than would be expected in single ring model compounds such as 2,4,6-triphenylpyrylium hydrogen sulfate (Figure S1). Therefore we suggest that C-O^+ stretch contributes to the 1590 v_{max}/cm^{-1} band in the spectra of the 500°C biochars. Although, we cannot unequivocally prove that C-O^+ stretch contributes to the 1590 v_{max}/cm^{-1} band, this assignment is consistent with the electronic environment of condensed aromatic structures found in biochar, the prominence of the peak 1590 v_{max}/cm^{-1} in the spectra, and the high levels of O present in the samples.

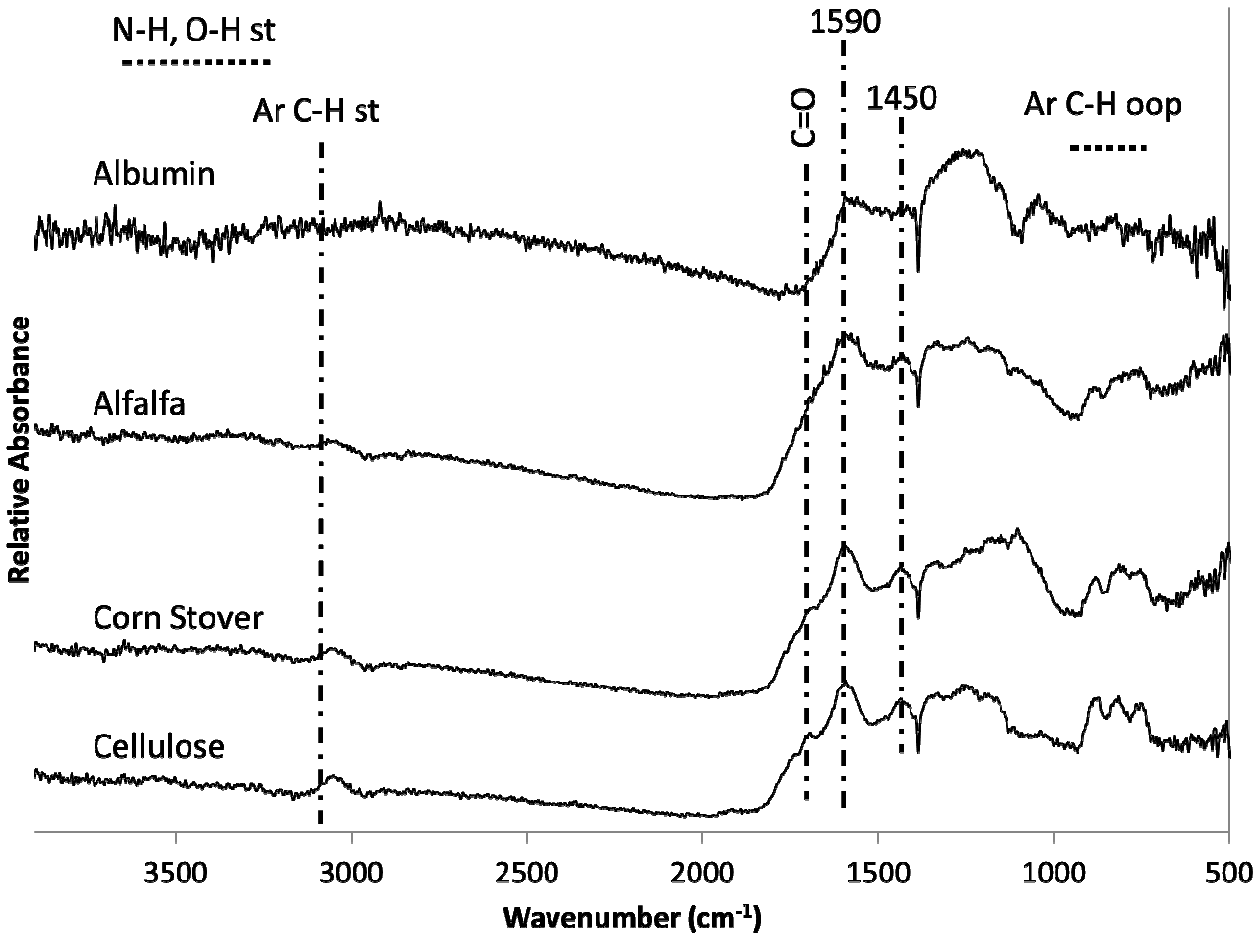

Figure 3. FTIR spectra of HCl treated 500 °C HTT biochars. N-H, O-H st indicate hydroxyl or amine/amide H-stretching; Ar C-H st is aromatic C-H stretching, C=O is carbonyl stretching, and Ar C-H oop indicates aromatic C-H out of plane vibration.

Intensities of all bands in the infra-red spectra of the 700 °C HTT biochars are much lower than in the spectra of the 500 °C HTT biochars. Changes in dipoles due to the absorption of infrared radiation are restricted in condensed aromatic structures. Thus the loss of intensity and the broadening of the absorption bands in addition to decreased H and N contents (Table 2) support the interpretation of increased condensation of aromatic carbon in the 700 °C HTT biochars relative to the 500 °C HTT biochars. The spectra of the HCl / HF treated 700 °C HTT biochars (Figure 4) exhibited a broad band ranging from 1400 to 1600 v_{max}/cm^{-1}, which we infer to be due to both aromatic C-C and C-heteroatom stretching. The 700 °C HTT cellulose biochar contained 6.12 % O (Table 2) but the FTIR spectra showed no hydroxyl bands and only weak carbonyl bands. The splitting of the carbonyl peak and its broad breadth in the spectra of the 700 °C HTT biochars (Figure 4) is indicative of Fermi resonance; indicating that multiple carbonyls are present within the same conjugated structure. The acid treatments caused apparent changes in the albumin biochars as manifested by increased alcohol character and declined intensity of the peak at 2170 v_{max}/cm^{-1} (Figures 2, 3, 4 & S1). The broad band observed in the spectrum of HCl / HF treated 700 °C HTT albumin biochar spanning from 2500 to 3500 v_{max}/cm^{-1}

is likely due to hydroxyl stretch perturbed by a broad range of electronic environments. This band is not observed in the dialyzed 700 °C HTT albumin biochar (Figure S1) and is therefore a result of oxidation during the acid treatments. For this reason, the structural O content of the HCl / HF treated albumin biochars reported previously is assumed to be higher than the structural O content of the fresh albumin biochars.

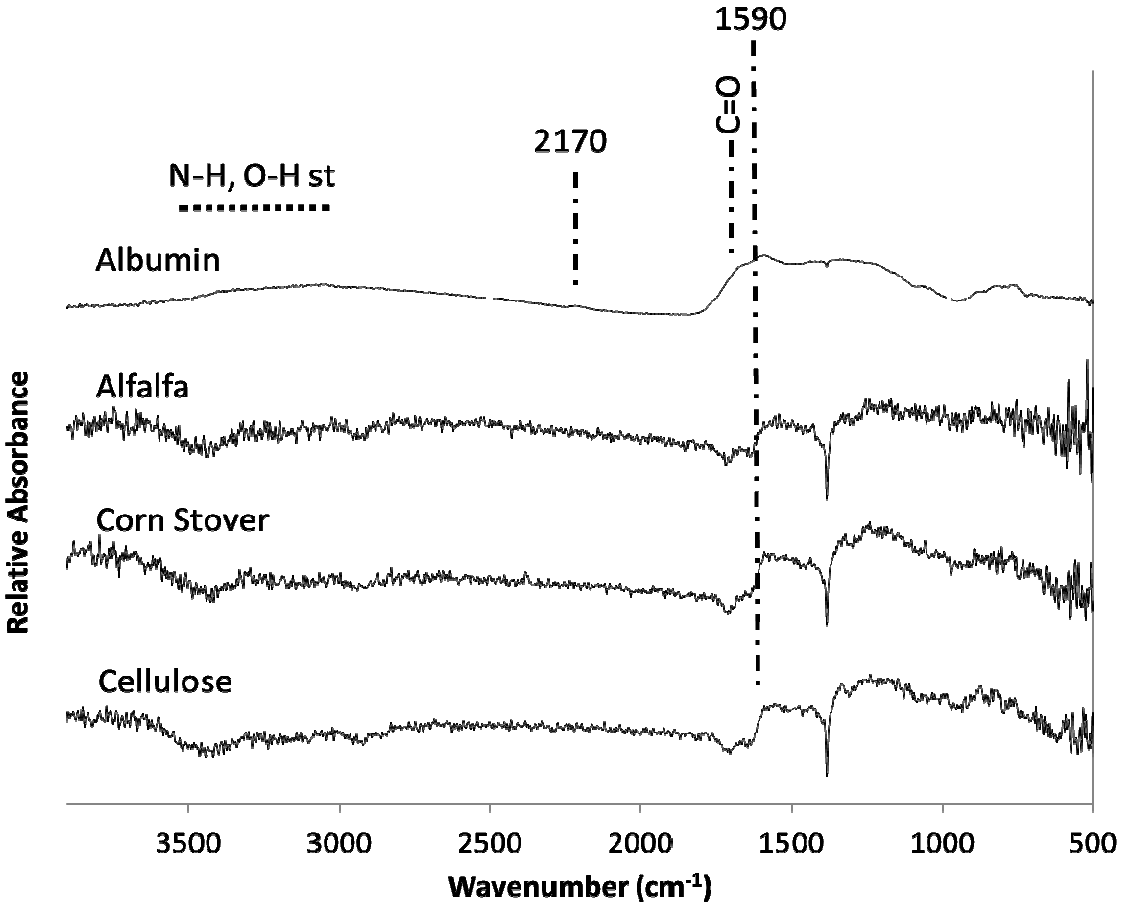

Figure 4. FTIR spectra of HCl / HF treated 700 °C biochars. N-H, O-H st indicate hydroxyl or amine/amide H-stretching; C=O indicates carbonyl stretching.

3.3 X-ray photoelectron spectroscopy

X-ray photoelectron spectroscopy provided additional evidence of oxonium heterocycles in biochar. The C1s spectra of biochars in addition to that of graphite and a model compound; 2,4,6-triphenylpyrylium hydrogen sulfate, are presented in Figure 5. The large peak at 285.0 ± 0.3 eV in the graphite and 2,4,6-triphenylpyrylium sulfate is attributed to aromatic C which is the dominant form of C in both of these reference compounds. The small shoulder from 286.7 eV to 288.5 eV evident in the C1s spectrum of 2,4,6 triphenylpyrylium sulfate is attributed to C bound to O^+, the only other form of C present in this reference compound. A broad shoulder in this region was also observed in the C1s spectrum of the 700°C HTT maize stover biochar. Background

intensity in this region but no distinct peak was observed in the spectra of the other biochars. Greater relative signal intensity in the 286.7 eV to 288.5 eV range in the C1s spectra was observed for biochars with greater AEC (Table 1).

The O1s spectrum of 2,4,6-triphenylpyrylium hydrogen sulfate displays two broad peaks representing pyrylium O and sulfate O. In the O1s spectrum, oxonium heterocycle O is assigned to the peak ranging from 534.0 to 536.6 eV. The broad O1s spectra (530 to 537 eV) for the graphite and various biochars indicate that multiple forms of O are present. Much of the O1s signal in the spectra of graphite and the biochars represents O with lower binding energies consistent with neutral and negatively charged O containing organic functional groups. However, the O1s spectra for the graphite and all of the biochars have some intensity between 534.0 to 536.6 eV, which is consistent with electron deficient oxonium groups. In general, the signal intensity in the oxonium region increased with the AEC (Table 1) of the studied biochars. Surprisingly, almost half of the O1s signal in the graphite spectrum was in the oxonium region. The graphite employed in this study was cleaved from an old monochromator which had been exposed to atmospheric oxygen and ionizing radiation.

Deconvolution of the N1s spectra revealed 69% N as pyridine-N (6 member N heterocycles) and 31% N as pyrrole (5 member N heterocycle) and pyridone (6 member N heterocycles with an amide group) in the 500 ˚C HTT albumin biochar and 58% N as pyridine-N and 42% N as pyrrole + pyridone-N in the 700 ˚C HTT albumin biochar (Figure 6). These findings suggest that pyridinal structures form at lower pyrolysis temperatures and are less heat resistant than pyrrole / pyridone structures. It should be noted that specific amino acids preferentially form 5 or 6 member N heterocycles during pyrolysis and therefore the types of N heterocycles found in a biochar are a function of protein composition of the feedstock as well as pyrolysis temperature[20].

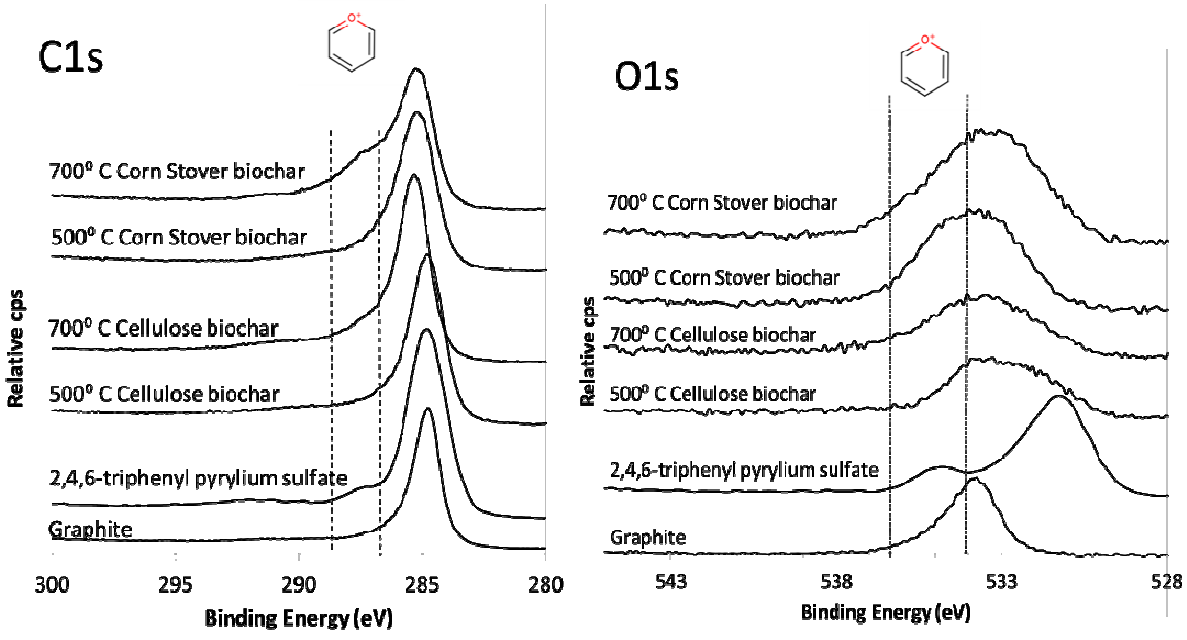

Figure 5. XPS spectra of C and O for untreated biochars, 2,4,6-triphenyl pyrylium sulfate, and graphite.

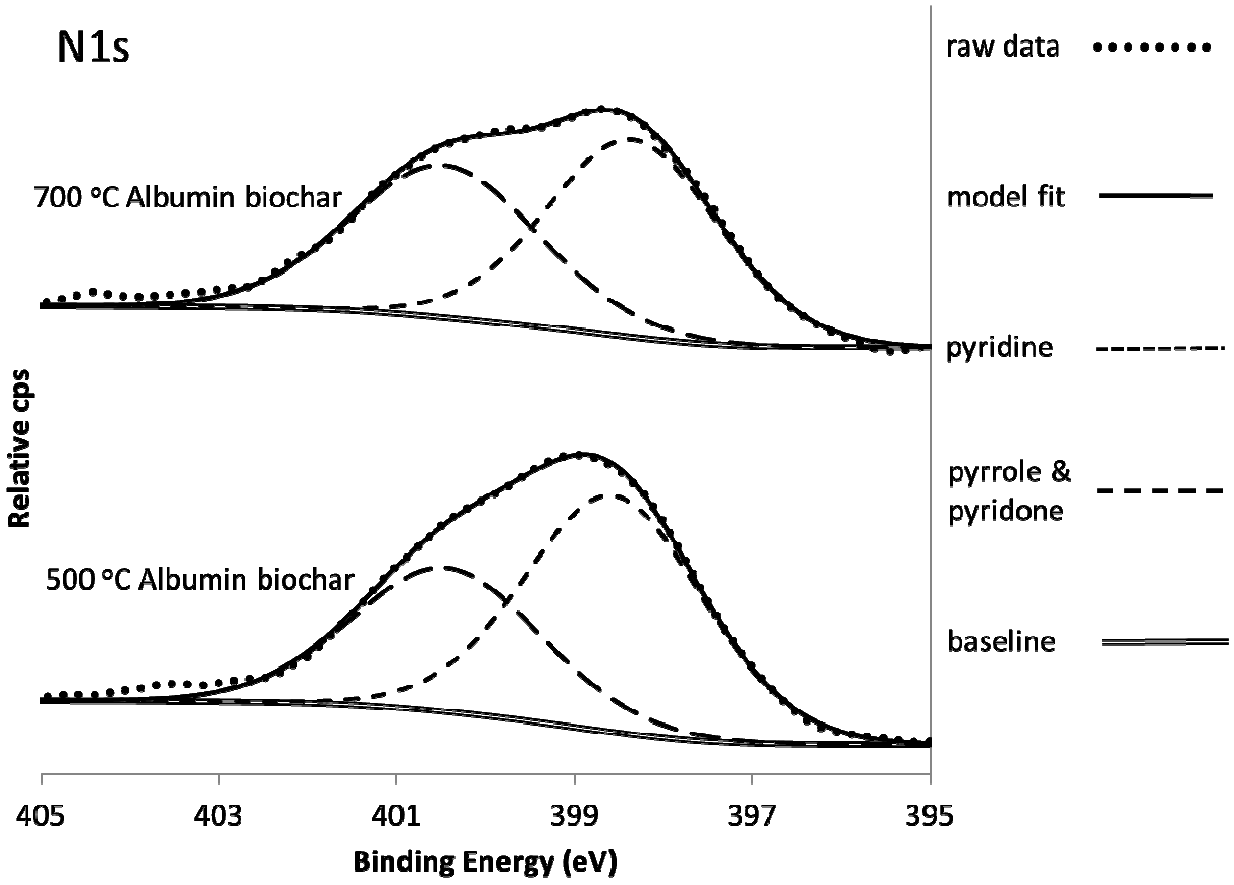

Figure 6. The N1s XPS spectra of the 500°C and 700°C albumin biochars.

4. Conclusions

We report significant AEC for biochars produced from four different feedstocks and that biochars equilibrated at pH 4 have substantially higher AEC values than biochars equilibrated at pHs 6 or 8. We have considered three possible sources for the origin of AEC in the studied biochars; pyridinium groups, oxonium groups, and protonated aromatic rings. The strong effect of pH on AEC of biochars is consistent with pyridinium groups and protonation of aromatic rings and the N1s XPS spectra of albumin biochars shows clear evidence of pyridinium groups. Neither of these mechanisms, however, can explain non-zero levels of AEC measured at pH 8. This observation can only be explained by the presence of pH independent oxonium groups. The contribution of oxonium groups to the AEC of the studied biochars is further supported by chemical evidence for the presence of substantial amounts of structural O in the biochars, FTIR spectra exhibiting a prominent 1590 cm^{-1} peak, which is consistent with C-O^{+} stretching in oxonium heterocycles, and interpretation of C1s and O1s x-ray photoelectron spectra. Therefore, we conclude that oxonium groups are present in biochars and contribute some of the measured AEC.

Acknowledgements

We extend our appreciation to Wenyu Huang, Scott Schlorholtz, Warren Straszheim, and Walter Trahanovsky of Iowa State University and Jim Anderegg of the Ames Laboratory for their various contributions to this work.

Funding Sources

This project was supported by Agriculture and Food Research Initiative Competitive Grant no. 2011-68005-30411 from the USDA National Institute of Food and Agriculture and by the National Science Foundation under Grant Number EPS-1101284.

Notes and references

Electronic Supplementary Information (ESI) available: [details of any supplementary information available should be included here]. See DOI: 10.1039/b000000x/

1 D. A. Laird, *Agron. J.,* 2008, **100,** 178-181.

2 D. A. Laird, P. D. Fleming, D. D. Davis, R. Horton, B. Wang, and D. L. Karlen, *Geoderma*, 2010, **158**, 443-449.

3 O. A. Knowles, B. H. Robinson, A. Contangelo, L. Clucas, *Sci. Total Environ.*, 2011, **409,** 3206-3210.

4 C. J. Mikan, M. D. Abrams, *Can. J. For. Res.*, 1996, **26,** 1893-1898.

5 B. Glaser, J. Lehmann, W. Zech, *Biol. Fertil. Soils*, 2002, **35**, 219-230.

6 D. W. van Krevelen, *Fuel*, 1950, **29,** 269-84.

7 C. E. Brewer, K. Schmidt-Rohr, J. A. Satrio, R. C. Brown, *Environ. Prog. Sustainable Energy*, 2009, **28:3,** 386-396.

8 X. Li, Q. Shen, D. Zhang, X. Mei, W. Ran, Y. Xu, Y. Guanghui, *PLoS ONE*, 2013, **8:6** e65949**,** doi:10.1371/journal.pone.0065949.

9 P. L. Ascough, M. I. Bird, P. Wormald, C. E. Snape, D. Apperley D, *Geochim. Cosmochim. Acta*, 2008, **72**, 6090-6102.

10 P. L. Ascough, M. I. Bird, S. M. Francis, B. Thornton, A. J. Midwood, A. C. Scott, D. Apperley, *Geochim. Cosmochim. Acta,* 2011, **75**, 2361-2378.

11 H. P. Boehm, *Carbon*, 1994, **32:5**, 759-769.

12 A. Mukherjee, A. R. Zimmerman, W. Harris, *Geoderma*, 2011, **163**, 247-255.

13 M. B. Inyang, P. Gao, P. Pullammanappallil, W. C. Ding, A. R. Zimmerman, *Bioresour. Technol.,* 2010, **101**, 8868-8872.

14 A. Silber, I. Levkovitch, E. R. Graber, *Environ. Sci. Technol.,* 2010, **44**, 9318-9323.

15 C. H. Cheng, J. Lehmann, M. H. Engelhard, *Geochim. Cosmochim. Acta,* 2008, **72,** 1598-1610.

16 W. J. Huang, C. Y. Chen, M. Y. Peng, *Water SA*, 2004, **30:3**, 369-375.

17 M. Voll and H. P. Boehm, *Carbon*, 1970, **8**, 741-752.

18 M. Ahmad, A. U. Rajapaksha, J. E. Lim, M. Zhang, N. Bolan, D. Mohan, M. Vithanage, S. S. Lee and Y. S. Ok, *Chemosphere* 2014, **99**, 19-33.

19 L. March, *Advanced Organic Chemistry*, 3rd ed 1985.

20 L. I. Darvell, C. Brindley, X. C. Baxter, J. M. Jones and A. Williams A, *Energy Fuels*, 2012, **26**, 6482-6491.

21 Z. A. Mayer, Y. Eltom, D. Stennett, E. Schröder, A. Apfelbacher and A. Hornung, *Environ. Prog. Sustainable Energy*, 2013, doi 10.1002/ep 11788.

22 J. R. Pels, F. Kapteijn, J. A. Moulijn, Q. Zhu and K. M. Thomas, *Carbon,* 1995, **33:11**, 1641-1653.

23 A. B. Fuertes, M. Camps-Arbestain, M. Sevilla, J. A. Macia-Agullo, S. Fiol, R. Lopez, R. J. Smernik, W. P. Aikenhead, F. Arce and F. Macias, *Aust. J. Soil Res.*, 2010, **48**, 618-626.

24 A. V. Bridgwater, M. Meier and D. Radlein, *Org. Geochem.*, 1999, **30**, 1479-1493.

25 S. Suttiback, *Int. J. Biosci.,* 2013, **3:7**, 82-89.

26 X. Cao and W. Harris, *Bioresour. Technol.*, 2010, **101**, 5222-5228.

27 Y. Ying Yao, B. Gao, M. Inyang, A. R. Zimmerman, X. Cao X, P. Pullammanappallil and L. Yang, *Bioresour. Technol.,* 2011, **102**, 6273-6278.

28 A. T. Balabang, D. Mateescu and M. ELIA, *Tetrahedron*, 1962, **18**, 1083-1094.

29 Z. Yoshida, H. Sugimotoa and S. Yoneda, *Tetrahedron*, 1972, **28**, 5873-5881.

30 R. S. Swift, in: *SSSA Book Series: 5, Methods of soil analysis, Part 3- Chemical methods; Soil Science Society of America*, Madison, Wi 1996, ch. 35, p 1019.

31 E. Pretsch, P. Buhlmann and M. Badertscher, eds. In: *Structure determination of organic compounds: Tables of spectral data, 4th*, rev. ed.; Springer 2009; doi 10.1007/978-3-540-93810-1.